the limited and tunable lifetime of the hydrogen bonds, the material is always in its thermodynamically most favorable configuration and the reversibility of the bonding permits the material to immediately adjust its configuration to external stimuli.

The bulk viscoelastic properties of reversible polymers of the kind described above are of interest for possible applications as materials. For compounds **2a**, **2b**, and **3**, however, these properties were difficult to study because of the history-dependent phase behavior and the tendency of these compounds to crystallize. Therefore, we investigated the properties of compound **6** with siloxane spacers (Fig. 4). The synthesis makes use of a protected compound **4**, which is regarded as a useful synthon for a large number of structures.

Neat compound **6** (number-average molecular weight M_n of the monomer is 8×10^3) shows shear thinning and polymer-like viscoelastic behavior, whereas its synthetic precursor **5** behaves in a purely Newtonian fashion (Fig. 5). The zero shear viscosity of **6** at 30°C is 1000 times the viscosity of **5** and is comparable to the value for unfunctionalized poly(dimethylsiloxane) with $M_n = 3 \times 10^5$. The strong temperature dependence of the viscosity of **6** is ascribed to an increased rate of chain-breaking as well as to increasing the dissociation at higher temperatures. To our knowledge, the thermoplastic behavior of **6** is unprecedented for self-assembled structures.

We extended our study to reversible networks that are always in their thermodynamically determined architecture. Reversible polymer networks were obtained from trifunctional copolymers of propylene oxide and ethylene oxide by functionalization with (isocyanatomethyl) methylcyclohexylisocyanate, followed by reaction with methylisocytosine (Fig. 6). Compound **7** has a plateau modulus of 5×10^5 Pa (Fig. 7), six times the plateau modulus of covalently cross-linked copolymer **8**. The phase angle of **7** shows a frequency-dependent transition from purely viscous to viscoelastic behavior (Fig. 7), whereas **8** is viscoelastic across the whole frequency range. If we may assume that the relaxation of **7** is described by a pure Maxwell element, the relaxation time at 30°C, determined at a phase angle of 45°, is estimated to be 0.1 s. This value agrees with NMR experiments of the lifetime of dimers of **1** and the mechanical properties of linear polymers **6**.

The higher plateau modulus of **7** compared to **8** and the frequency dependence of **7** shows that the reversible cross-links in **7** behave like entanglements in an ordinary linear polymer. The reversibility of the hydrogen bonds allows the molecules of **7** to assemble into a more dense, thermodynamically determined network, whereas the cross-links in **8** are irreversibly formed to yield a kinetically determined network.

The polymers assembled by well-defined dimerization of the quadruple hydrogen-bonded ureido-pyrimidone functionality have unique features that distinguish them from existing systems. Because of the high association constant, the linear polymers **2a** and **3** have DPs far exceeding those of existing self-assembled systems based on less than four hydrogen bonds. Polymer-like behavior is thus observed even in semidilute solution. At the same time, the directionality of the interaction prevents microphase separation through crystallization in the bulk material or gel formation in solution. Particularly in the reversible networks, the absence of unspecific aggregation means that a high level of control over the network architecture is possible, because the degree of association, the degree of branching, and the distance between cross-links can all be tuned through chemical modification of the spacers and by variation of the hydrogen-bonding functionality. As a result, polymer networks can be developed with thermodynamically controlled architectures, for use in hot melts and coatings, where a reversible, strongly temperature-dependent rheology is highly desirable.

REFERENCES AND NOTES

1. C. Hilger, M. Dräger, R. Stadler, *Macromolecules* **25**, 2498 (1992).
2. A. Aggeli, *et al.*, *Nature* **386**, 259 (1997).
3. M. Möller, J. Omeis, E. Mühleisen, in *Reversible Polymeric Gels and Related Systems*, P. S. Russo, Ed. (ACS Symp. Ser. 350, American Chemical Society, Washington DC, 1987), chap. 7.
4. J.-M. Lehn, *Makromol. Chem. Macromol. Symp.* **69**, 1 (1993).
5. C. D. Eisenbach, A. Göldel, M. Terskan-Reinold, U. S. Schubert, *Macromol. Chem. Phys.* **196**, 1077 (1995).
6. C. Alexander, C. P. Jariwala, C.-M. Lee, A. C. Griffin, *Macromol. Symp.* **77**, 283 (1994).
7. P. Bladon and A. C. Griffin, *Macromolecules* **26**, 6604 (1993).
8. C.-M. Lee, C. P. Jariwala, A. C. Griffin, *Polymer* **35**, 4550 (1994).
9. C. B. St. Pourcain and A. C. Griffin, *Macromolecules* **28**, 4116 (1995).
10. C. P. Lillya *et al.*, *ibid.*, **25**, 2076 (1992).
11. Y. Ducharme and J. D. Wuest, *J. Org. Chem.* **53**, 5787 (1988).
12. C. Fouquey, J.-M. Lehn, A.-M. Levelut, *Adv. Mater.* **2**, 254 (1990).
13. M. Kotera, J.-M. Lehn, J.-P. Vigneron, *J. Chem. Soc. Chem. Commun.* **1994**, 197 (1994).
14. T. J. Murray and S. C. Zimmerman, *J. Am. Chem. Soc.* **114**, 4010 (1992).
15. Full experimental details of the crystal structure determination will be published elsewhere (F. H. Beijer, H. Kooijman, R. P. Sijbesma, E. W. Meijer, in preparation).
16. M. E. Cates, *Macromolecules* **20**, 2289 (1987).
17. Assuming that the association constant of functional groups is independent of DP, we derived the following equation:

$$DP = \frac{2 \cdot ([\mathbf{2}] + [\mathbf{1}])}{[\mathbf{1}] - \frac{1}{4K_{dim}}\left[1 - \sqrt{1 + 8K_{dim}([\mathbf{1}] + 2 \cdot [\mathbf{2}])}\right]}$$

where the brackets denote concentration. When an exponential relation between η_{sp} and DP is assumed, the values of K_{dim} and the exponent in DP that give the best fit to the data are $\eta_{sp} \approx (DP)^{0.78}$ and $K_{dim} = 2.2 \times 10^6$.
18. P. J. Flory, *Principles of Polymer Chemistry* (Cornell Univ. Press, Ithaca, NY, 1953).
19. We thank J. Palmen and M. van Gurp (DSM Research) for performing mechanical measurements. The x-ray structure determination of 2-butylureido-6-methyl pyrimidone was performed by H. Kooijman and A. L. Spek (Bijvoet Center for Biomolecular Research, Crystal and Structural Chemistry, Utrecht University).

22 April 1997; accepted 26 September 1997

Two-Dimensional Melting of an Anisotropic Crystal Observed at the Molecular Level

H. D. Sikes and D. K. Schwartz*

A distinctive two-dimensional (2D) melting transition occurring at nearly 100 degrees Celsius (°C) has been observed in Langmuir-Blodgett films by in situ atomic force microscopy (AFM). A 2D orthorhombic crystal phase melted to a 2D smectic phase at about 91°C. The smectic phase was characterized by 1D molecular periodicity with short-range correlations (about 40 angstroms). At 95°C, the smectic order melted to form a hexatic phase. Infrared spectroscopy measurements were consistent with the AFM observations. These observations support the dislocation-mediated melting scenario for an anisotropic 2D crystal predicted by Ostlund and Halperin. A longer wavelength height modulation was also observed in the smectic and hexatic phases.

In the late 1970s, Halperin, Nelson, and Young (*1*) built upon the ideas of Kosterlitz and Thouless (*2*) to describe melting in two dimensions. Before melting to an isotropic liquid, a hexagonal crystal was predicted to pass through an intermediate "hexatic" phase that retained the sixfold orientational order of the crystal without long-range translational order. The proposed mechanism for the crystal-to-hexatic transition was the unbinding of pairs of lattice dislocations with opposite Burger's vec-

Department of Chemistry, Tulane University, New Orleans, LA 70118, USA.

*To whom correspondence should be addressed.

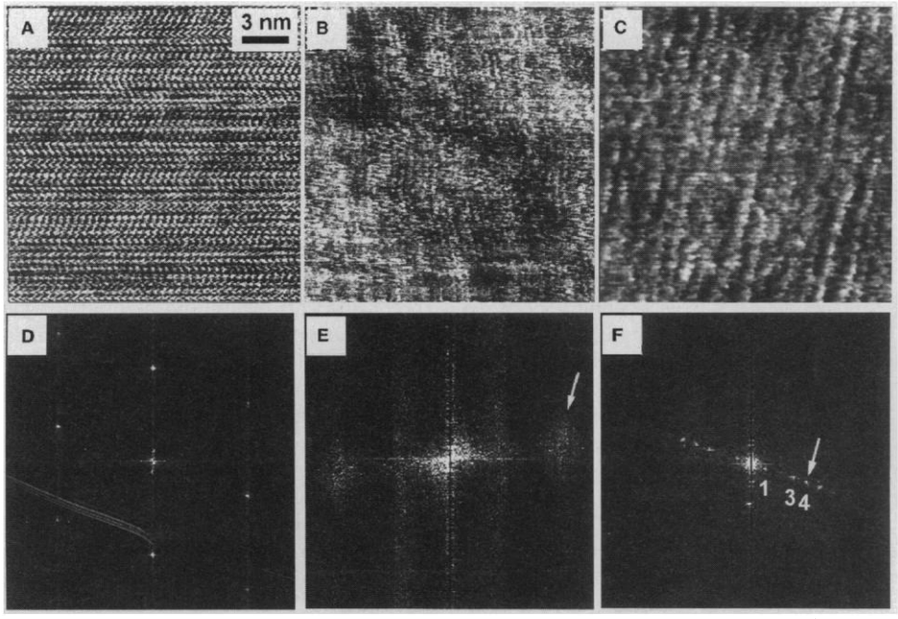

Fig. 1. Typical AFM images of cadmium arachidate trilayers at (**A**) 89°, (**B**) 93°, and (**C**) 95°, along with associated Fourier transforms (FTs) (**D**, **E**, and **F**, respectively) of larger regions surrounding the areas presented in the images. (A) The typical 2D molecular lattice for such films. The associated FT (D) displays three pairs of sharp spots corresponding to length scales of about 4 Å. The lattice is orthorhombic, so two pairs of spots correspond to a slightly larger repeat distance than the third pair. (B) The intermediate temperature image shows molecular-scale features running in lines. No true 2D lattice is observed, and the 1D periodicity is correlated only over small parts of the image. A longer wavelength height modulation is also faintly visible running in the same direction. The associated FT (E) shows a single pair of diffuse spots (corresponding to a length scale of about 4 Å) marked by an arrow. (C) At high temperature, no molecular-scale features are seen, only a 1D periodic modulation with a repeat distance of about 15 Å. The FT of the modulation (F) has spots in one direction only. The spot closest to the origin (labeled 1) corresponds to a superstructure with a repeat distance of four waves, a periodicity of 58 Å. The second harmonic is absent, but higher harmonics are observed. The fourth harmonic (labeled 4 and with an arrow) corresponds to the approximate separation of the clearly observed ripples in the image (15 Å).

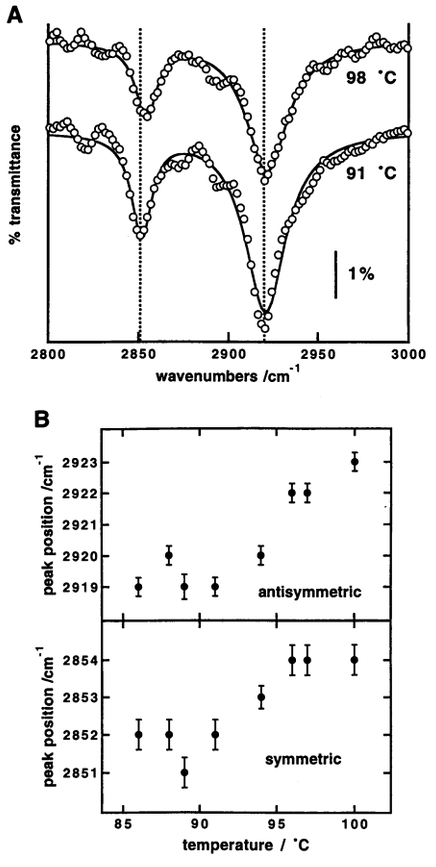

Fig. 2. (**A**) Transmission IR spectra (CH stretching region) of a CdA_2 LB multilayer as a function of temperature. The solid lines represent Lorentzian fits to the data. A small (about 3 cm^{-1}) but distinct shift of the peak positions to higher wave number is observed with increasing temperature, signaling a decrease in conformational order of the alkyl chains. The dashed lines are drawn at 2851 and 2920 cm^{-1}, respectively, as guides to the eye. (**B**) The peak position of the symmetric and antisymmetric methylene stretch bands as a function of temperature. Note that the peak positions at 94°C are at an intermediate position between low and high temperature values, consistent with an intermediate phase.

tors. A similar process was eventually observed in a colloidal crystal (*3*). However, despite the existence of a variety of hexatic phases in quasi-2D systems such as thin, freely suspended liquid-crystal films (*4*), Langmuir monolayers (*5*), and Langmuir-Blodgett (LB) films (*6*), this phase sequence has not been observed in a molecular system.

This absence likely arises from additional complications in systems of approximately cigar-shaped molecules, such as molecular tilt or anisotropic molecular cross section. In such cases, the crystal symmetry may be orthorhombic (rectangular) instead of hexagonal, and the six elementary dislocations will not be equivalent, but divided into groups of two (type I) and four (type II). Ostlund and Halperin (*7*) analyzed this situation and predicted that if the type I dislocations were to unbind first, a 2D smectic phase would be inserted into the phase diagram between the crystal and hexatic phases. The melting of an anisotropic 2D crystal to a 2D smectic would then be a signature of dislocation-mediated melting. We have directly observed the molecular details of this melting sequence in a LB film using AFM.

Previous infrared (IR) and Raman spectroscopy (*8*, *9*), electron diffraction (*10*), and x-ray scattering (*11*, *12*) studies of cadmium fatty-acid salt LB films demonstrated the existence of an order-disorder transition at high temperatures (the transition temperature was not determined precisely) in which the chains became less ordered and the local packing changed from orthorhombic to hexagonal. In the orthorhombic phase, the alkyl chains are organized in a "herringbone" arrangement; in the hexagonal phase, they rotate freely about their long axis. Because the correlation length in the hexagonal phase, determined by x-ray diffraction experiments (*12*), is only about 25 Å, this phase is actually hexatic. In previous AFM studies of low-temperature hexagonal rotator phases in LB films (*13*), we were unable to obtain molecular-resolution images (presumably because of the rapid molecular motion); the film surfaces appeared featureless and flat. This appearance was in contrast to LB films in crystalline phases, for which molecular resolution was routinely obtained (*13*, *14*). Therefore, the expected AFM signature of a crystal-to-hexatic phase transition was the reversible loss of molecular resolution. We used three-layer films for convenience; however, the melting was confined to the outer bilayer. The layer nearest the substrate has a disordered structure (*9*, *12*, *13*), even at low temperature; subsequent bilayers adopt the orthorhombic crystal symmetry.

We recorded high-resolution AFM images of cadmium arachidate (CdA_2) trilayers as a function of temperature (*15*, *16*)

(Fig. 1). Below 91°C, a well-ordered crystalline phase was observed (Fig. 1A). The molecular lattice was consistent with the previously observed centered rectangular (orthorhombic) structure (*13*). The digital Fourier transform (FT) of the image (Fig. 1D) shows three pairs of sharp first-order spots. Between 91° and 95°C, no true 2D lattice was observed, but molecular-sized features were still visible, running in "lines" (nearly vertical in Fig. 1B). In this 2D smectic phase, a longer wavelength height modulation was faintly visible in the same approximate direction. The lines of molecules meandered a bit and were not correlated beyond about 10 repeat distances. The FT (Fig. 1E) shows a pair of diffuse peaks (clouds of intensity) corresponding to this short-range, 1D periodicity. Above 95°C, no regular molecular-size features were observed (Fig. 1C), but the height modulation remained. Upon lowering the temperature, the sequence of phases was reversed. We did not observe phase coexistence at any temperature, consistent with continuous (not first order) phase transitions (dislocation-mediated melting theory predicts continuous phase transitions).

A 2D smectic phase is not expected to have long-range order in the same way as a 3D smectic. Toner and Nelson (*17*) noted that the effect of fluctuations and free dislocations is to destroy smectic order at length scales larger than a "dislocation correlation length" ξ_0. They describe the structure as blobs of smectic order with a typical dimension of ξ_0. On large length scales, the various blobs make up a nematic phase with a director defined as the average layer normal within each blob. We believe that our images of CdA_2 in the temperature range 91° to 95°C (Fig. 1B) are consistent with this picture. Small areas are observed where the smectic layering is well ordered. However, the phase of the layering is not correlated from blob to blob, and there is some dispersion in the direction of the layer normal across a given image. The broad peaks in the FT indicate the short-range nature of the correlations. A similar structure was observed at room temperature in a LB monolayer composed of disk-shaped molecules (*18*).

Transmission IR spectra of CdA_2 trilayers showed a small (about 3 cm^{-1}) but distinct blueshift in the positions of the methylene stretch bands in exactly the same temperature range (Fig. 2), consistent with increased chain disorder (*19*, *20*). This correspondence implies a coupling between the melting of the 2D crystallinity and the onset of conformational disorder in individual alkyl chains. Given the experimental uncertainties in the peak positions, it is difficult to determine whether the conformational disorder increases continuously or in steps corresponding to the structures observed with AFM.

The high-temperature height modulation in CdA_2 had an average repeat distance of 15 ± 1 Å. In particularly good images, a superstructure in the modulation was observed to repeat every four waves. The superstructure was characterized as a systematic variation in peak separation. The FT of the modulation (Fig. 1F) shows a fundamental peak (labeled 1) at a distance corresponding to the superstructure (about 58 Å). The second harmonic of this superstructure peak is missing, but higher harmonics are observed. The fourth harmonic (marked by an arrow) corresponds to the periodicity of the plainly visible ripples. We observed a related high-temperature modulation in the shorter chain cadmium palmitate ($CdPa_2$) LB films. A $CdPa_2$ trilayer (Fig. 3A) at 85°C shows a periodicity of 10 ± 1 Å; the transition temperature decreases with chain length as expected. However, the modulation in $CdPa_2$ had a qualitatively different appearance than that in CdA_2. In the shorter chain compound (Fig. 3A), the modulation was extremely well ordered and correlated and appeared to have a sawtooth cross section. However, the modulation in the longer chain compound (Fig. 1C) had a rounded cross section and was less well ordered, that is, numerous "dislocations" could be seen in large-scale images.

Although one should use caution in applying 2D theory to systems with nonzero thickness (*21*), our observations are consistent with theoretical predictions of 2D melting. Ostlund and Halperin (*7*) predicted that an orthorhombic 2D crystal should melt to a 2D smectic phase if the type I dislocations unbind before the type II dislocations. Interestingly, Tippmann-Krayer *et al.* (*12*) provided direct evidence from their x-ray scattering data of CdA_2 multilayers that the type I dislocations unbind first. At low temperatures, they observed two diffraction peaks: one corresponding to the (11) and ($1\bar{1}$) lattice planes (type II Burger's vectors), the other corresponding to the (02) lattice plane (type I Burger's vector). Even at room temperature, the (11) peak was narrower, corresponding to a correlation length of about 90 Å, whereas the correlation length in the (02) direction was about 60 Å. However, at 93°C, the correlation length in the (02) direction dropped precipitously to 30 Å (within experimental uncertainty of the correlation length in the high-temperature hexatic phase), whereas the correlation length in the (11) direction was 80 Å. We interpret this difference as direct evidence that the (02), or type I, dislocations unbind at a lower temperature than the degenerate (11), or type II, dislocations, consistent with our observation of a smectic phase.

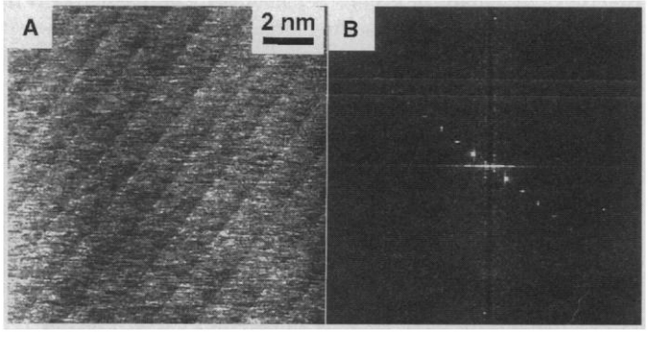

Fig. 3. (**A**) AFM image of a cadmium palmitate trilayer at 85°C along with (**B**) the associated FT of a larger region surrounding the region presented in the image. The image shows only 1D periodicity with a repeat distance of about 10 Å. The height modulation runs diagonally across the image and has a sawtooth height profile. The FT has spots only in one direction. The sharp spots and many harmonics demonstrates the high degree of correlation. Below about 80°C, a molecular lattice similar to that shown in Fig. 1A is observed.

REFERENCES AND NOTES

1. D. R. Nelson, *Phys. Rev. B* **18**, 2318 (1978); B. I. Halperin and D. R. Nelson, *Phys. Rev. Lett.* **41**, 121 (1978); D. R. Nelson and B. I. Halperin, *Phys. Rev. B* **19**, 2457 (1979); A. P. Young, *ibid.*, p. 1855.
2. J. M. Kosterlitz and D. J. Thouless, *J. Phys. C* **6**, 1181 (1973).
3. C. A. Murray, W. A. Sprenger, R. A. Wenk, *Phys. Rev. B* **42**, 688 (1990).
4. P. S. Pershan, *Structure of Liquid Crystal Phases*. (World Scientific, Singapore, 1988).
5. C. M. Knobler and R. C. Desai, *Annu. Rev. Phys. Chem.* **43**, 207 (1992).
6. S. Garoff, H. W. Deckman, J. H. Dunsmuir, M. S. Alvarez, *J. Phys. (Paris)* **47**, 701 (1986); R. Viswanathan, L. L. Madsen, J. A. Zasadzinski, D. K. Schwartz, *Science* **269**, 51 (1995).
7. S. Ostlund and B. I. Halperin, *Phys. Rev. B* **23**, 335 (1981).
8. J. P. Rabe, J. D. Swalen, J. F. Rabolt, *J. Chem. Phys.* **86**, 1601 (1987); L. Rothberg, G. S. Higashi, D. L. Allara, S. Garoff, *Chem. Phys. Lett.* **133**, 67 (1987); T. Hasegawa, S. Takeda, A. Kawaguchi, J. Umemura, *Langmuir* **11**, 1236 (1995).
9. M. Shimomura, K. Song, J. P. Rabolt, *Langmuir* **8**, 887 (1992).
10. C. Böhm, R. Steitz, H. Riegler, *Thin Solid Films* **178**, 511 (1989).
11. M. R. Buhaenko, M. J. Grundy, R. M. Richardson, S. J. Roser, *ibid.* **159**, 253 (1988); Y. Sasanuma, Y. Kitano, A. Ishitani, H. Nakahara, K. Fukuda, *ibid.* **199**, 359 (1991).
12. P. Tippmann-Krayer, R. M. Kenn, H. Möhwald, *ibid.*

210/211, 577 (1992).
13. D. K. Schwartz, J. Garnaes, R. Viswanathan, J. A. N. Zasadzinski, *Science* **257**, 508 (1992); D. K. Schwartz, J. Garnaes, R. Viswanathan, S. Chiruvolu, J. A. N. Zasadzinski, *Phys. Rev. E* **47**, 452 (1993).
14. J. Garnaes, D. K. Schwartz, R. Viswanathan, J. A. N. Zasadzinski, *Nature* **357**, 54 (1992).
15. Arachidic or palmitic acid (Sigma, >99%) LB multilayers were transferred to mica or thermally oxidized silicon substrates by the conventional vertical deposition method from a 0.5 mM $CdCl_2$ subphase (Millipore water was used), adjusted to pH = 6.5, and contained in a Nima (Coventry, England) LB trough. Imaging was performed with the use of a Nanoscope III Multimode atomic force microscope (Digital Instruments) in contact mode using a silicon nitride cantilever with integral tip. The equilibrium deflection of a given cantilever was quite sensitive to temperature; therefore, the tip was withdrawn before large temperature jumps and re-engaged after the temperature had stabilized. A small thermoelectric Peltier element (Melcor, Trenton, NJ) and a thermocouple (Omega Engineering, Stanford, CT) were sandwiched between a magnetic stainless steel base and a small piece of copper sheet and bonded together with thermally conductive epoxy. The entire assembly was less than 5 mm thick and 12 mm in cross section. Extremely thin and flexible electrical leads were carefully strain-relieved to avoid transmission of vibrations to the microscope. Over the usable temperature range of the device, 20° to 120°C, the scanner temperature remained below 35°C, minimizing difficulties associated with thermal drift. A previously reported temperature-controlled microstage (*16*) functioned only below 80°C. Several important control experiments were performed to validate the technique. Invariant molecular-resolution images of mica substrates were obtained to well above 100°C. High-resolution images of all three types of structure were quantitatively consistent after changing the scan size or rate, rotating the scan direction, or annealing at constant temperature for hours. The surface structure changed at the same temperature in nine separate repetitions of the experiment (using different samples and AFM tips) and reversibly changed back upon lowering of the temperature while using the same tip. On one occasion, we were even able to maintain the tip in contact with the film during this thermal cycling and continuously observed the loss and then reappearance of molecular order. These experiments prove that the loss of molecular resolution was due to increased molecular disorder, not degradation of a particular tip, and that the images represent structure indigenous to the sample, not related to temporal noise or induced by scanning.
16. I. Musevic, G. Slak, R. Blinc, *Rev. Sci. Instrum.* **67**, 2554 (1996).
17. J. Toner and D. R. Nelson, *Phys. Rev. B* **23**, 316 (1981).
18. J. Y. Josefowicz *et al.*, *Science* **260**, 323 (1993).
19. D. G. Cameron and R. A. Dluhy, in *Spectroscopy in the Biomedical Sciences*, R. M. Gendreau, Ed. (CRC Press, Boca Raton, FL, 1986), pp. 53–86.
20. Transmission IR spectra were recorded with the use of a Mattson Cygnus 100 spectrometer with a 6.4-mm pinhole defining the incident beam. The sample holder was heated using a thin film resistive heating element (Minco, Minneapolis, MN); the temperature was measured with a thermocouple (Omega). After obtaining the multilayer spectrum, the sample holder was removed and placed in an ultraviolet-oxygen cleaner (Boekel Industries, Feasterville, PA), where the film on both sides of the substrate was removed. The holder was then repositioned within the spectrometer, to within 0.1 mm of the original position, and the background spectrum was measured.
21. C.-Y. Chao, C.-F. Chou, J. T. Ho, A. Jin, C. C. Huang, *Phys. Rev. Lett.* **77**, 2750 (1996).
22. We thank D. R. Nelson for his helpful comments regarding 2D melting. This work was supported by the National Science Foundation (NSF), the donors of the Petroleum Research Fund, and the Center for Photoinduced Processes (funded by NSF and the Louisiana Board of Regents).

5 May 1997; accepted 17 October 1997

Enhanced Intergrain Tunneling Magnetoresistance in Half-Metallic CrO_2 Films

H. Y. Hwang and S.-W. Cheong

Low-field tunneling magnetoresistance was observed in films of half-metallic CrO_2 that were grown by high-pressure thermal decomposition of CrO_3. High-temperature annealing treatments modified the intergrain barriers of the as-grown films through surface decomposition of CrO_2 into insulating Cr_2O_3, which led to a threefold enhancement of the low-field magnetoresistance. This enhancement indicates the potential of this simple method to directly control the interface barrier characteristics that determine the magnetotransport properties.

Half-metallic ferromagnets exhibit conducting states at the Fermi level (E_F) for majority-spin electrons, but a semiconductor gap for minority-spin electrons (*1*). The resulting high degree of spin-polarization of Fermi-level electrons suggests that this class of materials could exhibit enhanced spin-dependent magnetotransport. Transition metal oxides can exhibit half-metallic behavior, in part because of their narrow conduction bands derived from transition metal *d* levels and oxygen *p* levels. Recently, low-field spin-polarized tunneling magnetoresistance (MR) was observed in polycrystalline perovskite manganites, layered manganites, artificial thin-film trilayer structures of perovskite manganites, and polycrystalline pyrochlore $Tl_2Mn_2O_7$, all of which are (or are suspected to be) half-metallic ferromagnets (*2–6*). In another example, perovskite manganite electrodes were used to inject spin-polarized carriers into a high-temperature superconductor, which suppressed the critical current by pair breaking (*7*).

All of the oxide systems currently investigated for tunneling MR are Mn-based, although this phenomenon should not be specific to the manganites. Half-metallic ferromagnetism has been suspected in the technologically important CrO_2. Already a staple magnetic recording medium, band structure calculations of CrO_2 predict 100% spin polarization at E_F (*8*). Spin-polarized photoemission and vacuum tunneling experiments show nearly complete spin polarization 2 eV below E_F, but a negligible density of states at E_F, inconsistent with metallic behavior (*9*, *10*). Because CrO_2 has a higher Curie temperature (T_C = 395 K) than all of the aforementioned systems and is already processed in large volumes in industry, it is a promising material in which to explore tunneling MR.

Previous studies of single-crystal CrO_2 report little MR below T_C, but in analogy to a recent comparison of single crystal and polycrystalline perovskite manganites, polycrystalline CrO_2 might exhibit low-field intergrain tunneling MR (*3*). We studied polycrystalline CrO_2 films grown by high-pressure thermal decomposition of CrO_3 on $SrTiO_3$ substrates and observed significant low-field spin-polarized tunneling MR at low temperatures in as-grown films. High-temperature annealing treatments significantly enhance low-field MR by modification of the effective intergrain tunneling barrier through surface decomposition of CrO_2 into insulating Cr_2O_3. This method provides a convenient way to control the interface properties for tunneling MR.

We prepared polycrystalline films of CrO_2 by dissolving CrO_3 powders in deionized water. The solution was uniformly applied on single-crystal $SrTiO_3$ substrates. Curing the specimen in a dry-air atmosphere removed the water and left a thin layer (typically a few micrometers) of polycrystalline CrO_3. Treatment in a few hundred bars of oxygen pressure with increasing temperature led to a series of decomposition reactions $CrO_3 \rightarrow (Cr_3O_8 \rightarrow Cr_2O_5) \rightarrow CrO_2 \rightarrow Cr_2O_3$, which are very sensitive to the applied temperature and pressure (*11*). Furthermore, only under high oxygen pressure does a narrow but distinct temperature window exist for stable, single-phase CrO_2. Because CrO_2 is metallic whereas CrO_3 and Cr_2O_3 are insulating, monitor-

H. Y. Hwang, Bell Laboratories, Lucent Technologies, Murray Hill, NJ 07974, USA.
S.-W. Cheong, Bell Laboratories, Lucent Technologies, Murray Hill, NJ 07974, and Department of Physics and Astronomy, Rutgers University, Piscataway, NJ 08855, USA.